Figure 2. Naito et al.

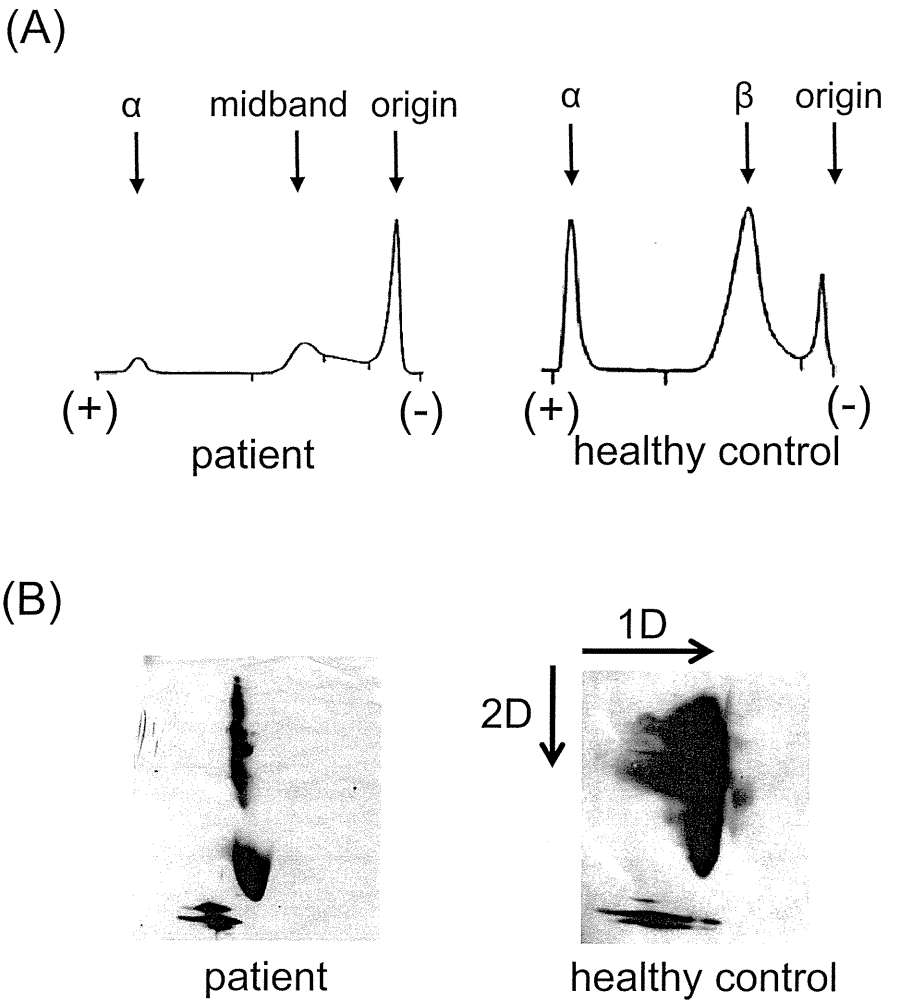

Figure 3. Naito et al.

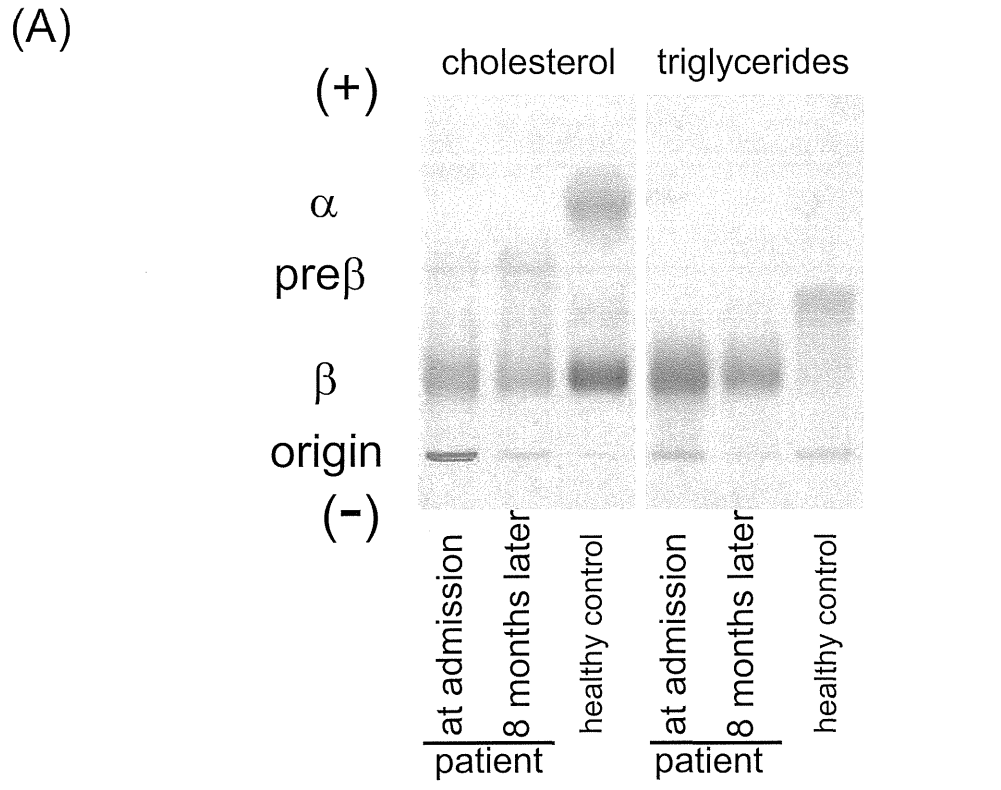

Lipid fraction		Normal value	At admission	At 8 months of treatment
total cholesterol	(mg/dl)	120-220	235	80
triglyceride	(mg/dl)	30-150	235	142
LDL-cholesterol	(mg/dL)	70-139	39	33
HDL-cholesterol	(mg/dL)	40- 96	22	19
free cholesterol	(mg/dL)	30- 65	205	71
cholesterol ester	(mg/dL)	90-200	30	9
free/total cholesterol	(%)	70-80	87	88

Table 1.

Lipid profiles in a patient with LCAT deficiency following a fat-restriction diet and administration of losartan for 8 months

Lipid profiles at admission and after adoption of a fat-restriction diet consisting of 10 g fat, 45 g protein and 1570 kcal energy per day and administration of losartan 50 mg for 8 months on lipid profile in a patient with LCAT deficiency.

Apolipoprotein fraction		Normal values	At admission	After 8 months of treatment
apoA-I	(mg/dL)	126 - 165	39	34
apoA-II	(mg/dL)	24 - 33.3	5.1	3.3
apoB	(mg/dL)	66 - 101	63	55
apoC-II	(mg/dL)	1.5 - 3.8	5.6	1.3
apoC-III	(mg/dL)	5.4 - 9.0	8.6	3.5
apoE	(mg/dL)	2.8 - 4.6	10.8	5.4

Table 2. Apolipoprotein profile in a patient with LCAT deficiency before and after treatment with a fat-restriction diet and administration of losartan for 8 months
Apolipoprotein profile at admission, and effect of a fat-restriction diet consisting of 10 g fat, 45 g protein, and 1570 kcal energy per day for 8 months on apolipoproteins in a patient with LCAT deficiency.

EXPERIMENTAL and MOLECULAR MEDICINE, Vol. 44, No. 5, 330-339, May 2012

Platelet-rich plasma inhibits the apoptosis of highly adipogenic homogeneous preadipocytes in an *in vitro* culture system

Yoshitaka Fukaya[1], Masayuki Kuroda[2,3,6], Yasuyuki Aoyagi[2,3], Sakiyo Asada[2,3], Yoshitaka Kubota[1], Yoshitaka Okamoto[2], Toshinori Nakayama[4], Yasushi Saito[5], Kaneshige Satoh[1] and Hideaki Bujo[3]

[1]Department of Plastic and Reconstructive Surgery
Graduate School of Medicine
Chiba University
Chiba 260-0856, Japan
[2]Center for Advanced Medicine
Chiba University Hospital
Chiba 260-0856, Japan
[3]Department of Genome Research and Clinical Application
[4]Department of Immunology
Graduate School of Medicine
Chiba University
Chiba 260-0856, Japan
[5]Chiba University
Chiba 260-0856, Japan
[6]Corresponding author: Tel, 81-43-222-7171;
Fax, 81-43-226-8130; E-mail, kurodam@faculty.chiba-u.jp
http://dx.doi.org/10.3858/emm.2012.44.5.037

Accepted 7 February 2012
Available Online 8 February 2012

Abbreviation: BIM, Bcl-2-interacting mediator of cell death

Abstract

Auto-transplantation of adipose tissue is commonly used for the treatment of tissue defects in plastic surgery. The survival of the transplanted adipose tissue is not always constant, and one of reasons is the accelerated apoptosis of the implanted preadipocytes. We have recently established highly homogeneous preadipocytes, named ccdPAs. The aim of the current study was to evaluate the regulation of the potency of platelet-rich plasma (PRP) on the apoptosis of ccdPAs *in vitro*. PRP stimulated the proliferation of the preadipocytes in a dose-dependent manner, and the stimulatory activity of 2% PRP was significantly higher than that of 2% FBS or 2% platelet-poor plasma (PPP). The presence of 2% PRP significantly inhibited serum starvation- or TNF-α/cycloheximide-induced apoptosis in comparison to 2% FBS or 2% PPP. DAPK1 and Bcl-2-interacting mediator of cell death (BIM) mRNAs were reduced in the preadipocytes cultured with 2% PRP in comparison to those cultured in 2% FBS. The gene expression levels were significantly higher in cells cultured without serum in comparison to cells cultured with 2% FBS, and the levels in the cells with 2% PRP were reduced to 5-10% of those in the cells without serum. These results indicated that ccdPAs exhibit anti-apoptotic activities, in addition to increased proliferation, when cultured in 2% PRP in comparison to the same concentration of FBS, and that this was accompanied with reduced levels of DAPK1 and BIM mRNA expression in *in vitro* culture. PRP may improve the outcome of transplantation of adipose tissue by enhancing the anti-apoptotic activities of the implanted preadipocytes.

Keywords: adipocytes; apoptosis; Bcl-2-like protein 11; death-associated protein kinase; platelet-rich plasma; tissue transplantation

Introduction

Aspirated fat is a common source of autologous tissue transplantation for the correction of tissue defects in plastic and reconstructive surgery (Billings and May, 1989; Patrick, 2000, 2001). Aspirated fat contains multipotential preadipocytes and progenitor cells, which have been utilized as a source of cell-based regenerative medicine (Stashower *et al.*, 1999; Zuk *et al.*, 2001; Gimble *et al.*, 2007; Yoshimura *et al.*, 2009; Bauer-Kreisel *et al.*, 2010; Sterodimas *et al.*, 2010). Although several different techniques of fat grafting have been developed, the outcomes of the transplantation vary widely. The most important factor required for successful grafting is to optimize the survival of the transplanted preadipocytes and other cells in the graft. In previous studies, we and others have shown that various cytokines are involved in the efficient cell survival of the implants (Kimura *et al.*, 2003;

Copyright © 2012 by the Korean Society for Biochemistry and Molecular Biology
This is an open-access article distributed under the terms of the Creative Commons Attribution Non-Commercial License (http://creativecommons.org/licenses/by-nc/3.0) which permits unrestricted non-commercial use, distribution, and reproduction in any medium, provided the original work is properly cited.

Yamaguchi *et al.*, 2005; Cho *et al.*, 2006; Torio-Padron *et al.*, 2007; Kuramochi *et al.*, 2008; Ning *et al.*, 2009).

Platelet rich plasma (PRP) (Eppley *et al.*, 2006; Foster *et al.*, 2009; Redler *et al.*, 2011) has been widely applied for practical medicine, such as aesthetic plastic surgery and the treatment of soft-tissue ulcers (Welsh, 2000; Man *et al.*, 2001; Margolis *et al.*, 2001; Bhanot and Alex, 2002; Martinez-Zapata *et al.*, 2009; Sclafani, 2009). Once activated, platelets secrete various bioactive cytokines, including platelet-derived growth factor (PDGF) and transforming growth factor beta 1 (TGF-β1), which increase angiogenesis and cell proliferation relevant to soft tissue regeneration. PRP has been applied for fat grafting, and in fact, has been shown to improve the survival of implanted adipose tissue in patients (Abuzeni and Alexander, 2001; Sadati *et al.*, 2006; Cervelli *et al.*, 2009). Thus, the use of PRP has been broadened to the tissue-engineering field using adipose tissue-derived multi-potential cells (Anitua *et al.*, 2006; Muller *et al.*, 2009). PRP is also expected to function as an autologous fibrin-based scaffold for transplanted cells (Anitua *et al.*, 2006; Wu *et al.*, 2009; Kang *et al.*, 2011). In fact, recent our study showed that fibrin-based scaffold decreased the apoptotic cell death of murine ccdPAs in mice transplantation model (Aoyagi *et al.*, 2011).

We have recently identified proliferative preadipocytes, ceiling culture-derived proliferative adipocytes (ccdPAs), as homogeneous cells suitable for *ex vivo* gene therapy applications *via* autologous transplantation (Asada *et al.*, 2011; Kuroda *et al.*, 2011). The ccdPAs are characterized by their high proliferative capacity with spontaneous adipogenic potential in scaffold fibrin gel culture (Aoyagi *et al.*, 2012). The establishment of a highly homogenous preadipocyte line made it possible to perform examinations to identify the optimal scaffolds and cytokines that can be used to improve the survival of transplanted preadipocytes. We herein studied the effects of PRP, and an autologous cytokine cocktail, on the apoptotic properties of preadipocytes using the ccdPAs.

Results

PRP inhibits fibrin scaffold gel shrinkage and improves the viability of ccdPAs in 3-dimensional culture

We have recently established a 3-dimensional (3-D) culture system for ccdPAs using fibrin gel (FG) (Aoyagi *et al.*, 2012). Using the 3-D culture system, the effects of PRP on the gel shrinkage and cell viability were analyzed in comparison to FBS. The FG/ccdPAs were formed and maintained in culture medium containing 10% FBS for 16 hr. The culture medium was replaced with fresh medium containing 2% PRP, 2% FBS or 10% FBS, or with medium without serum, and cells were subsequently incubated for an additional 24 hr.

The resulting gel sizes varied among the cultures grown in each type of medium. The gels without serum or with 2% FBS showed a drastic volume reduction, while the volumes of the gels cultured with 10% FBS or 2% PRP were not obviously reduced (Figure 1A). The culture supernatants were collected from each well and LDH activity was measured to evaluate the viability of cells. The LDH activity significantly decreased in the culture medium with 2% PRP in comparison to the medium with 2% or 10% FBS (Figure 1B). TUNEL staining of the gel sections showed the number of apoptotic cells to significantly decrease in the medium with 2% PRP in comparison to the medium with 2% FBS (1.5 ± 1.1% vs 9.8 ± 1.9%, $P < 0.05$). These results suggested that 2% PRP inhibits the shrinkage of FG/ccdPAs gels, and improves the cell viability in comparison to the same concentration of FBS.

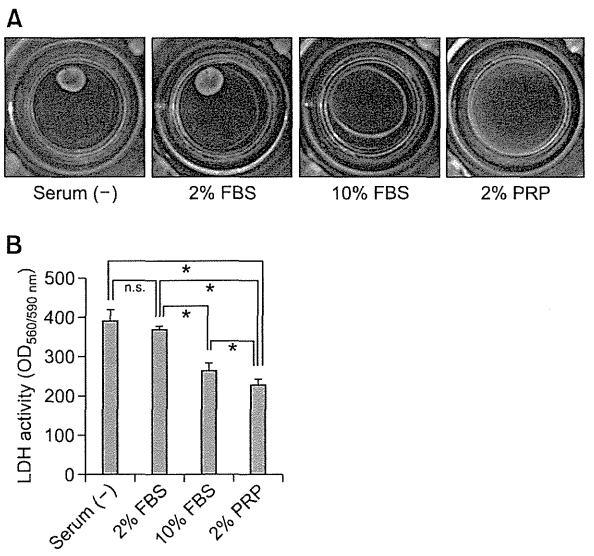

Figure 1. The effects of platelet-rich plasma (PRP) on the 3-dimensional culture of ccdPAs. 100 μl of fibrin gels containing 1×10^7 cells/ml of ccdPAs (FG/ccdPAs) were formed in cell culture insert and incubated in DMEM/HAM with 10% FBS for 16 hrs. The medium was replaced by DMEM/HAM in the presence or absence of different concentrations of FBS or PRP. (A) Photographs of FG/ccdPAs in the inserts were taken after 24 hr of culture. (B) The culture supernatant was collected from each well and the LDH activities expressed by the fluorescence of resorufin generated by coupled enzymatic reaction were examined. *$P < 0.05$.

PRP has a high proliferation-inducing potential for ccdPAs in plate culture

In order to evaluate the function of PRP on cell survival in the gel, we next examined the effects of PRP on the proliferation of ccdPAs in comparison to FBS. The cells (2.5×10^5 cells) were seeded and incubated with DMEM/HAM containing 20% FBS in 10 cm dishes for 16 hr. The media was replaced with medium containing 2% PRP, 2% FBS, or 10% FBS, and the cells were then cultured for 3 days. The cell appearance was not apparently changed among the ccdPAs cultured for 3 days in plates with media containing 2% PRP, 2% FBS, or 10% FBS (Figure 2A). To examine the cell proliferation, 2×10^3 cells of ccdPAs were seeded onto 96 well plates and incubated at 37°C for 24 hr. The media was replaced with medium with or without 2% PRP, 2% FBS, or 10% FBS (Day 0), and the cells were cultured for 3 days. The number of cells in each well was evaluated by measuring the DNA content. In contrast to the observation that the cell numbers on Day 3 were not significantly changed in comparison to those at Day 0 in the cultures incubated in medium containing 2% FBS, the cell numbers were significantly increased in cells cultured in the medium with 10% FBS or 2% PRP, and notably, the number of cells on Day 3 in the medium containing 2% PRP was significantly increased in comparison to the cells cultured with 10% FBS (Figure 1B). The cell numbers in the media with various concentrations of PRP showed a dose-dependent increase up to 5% PRP; the number of cells present in the media with 0.5-1% PRP was almost equivalent to that of the cells cultured with 5-10% FBS (Figure 2C). These results indicated that the proliferation-inducing potential of PRP for ccdPAs was higher in comparison to that of FBS.

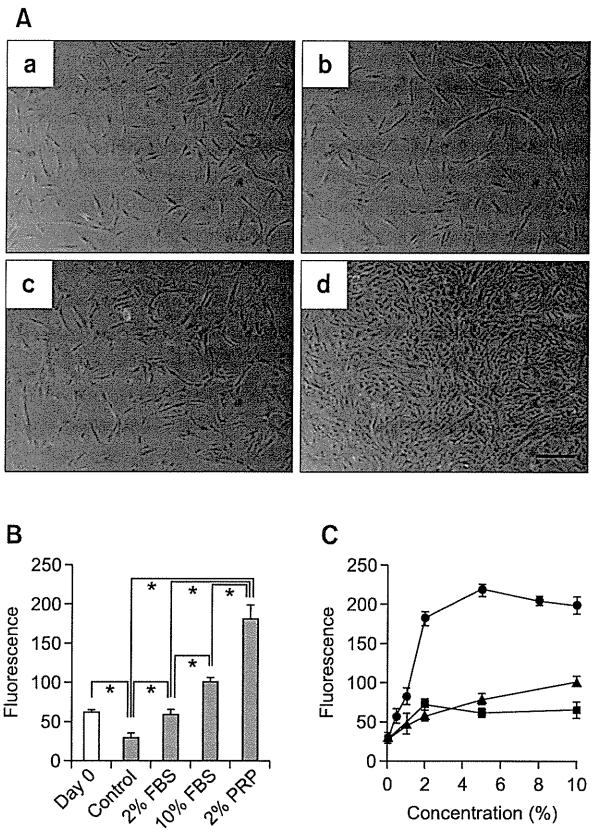

Figure 2. Platelet-rich plasma (PRP) promotes the proliferation of ccdPAs. (A) Photographs of ccdPAs were taken after 3 days in culture containing DMEM/F12-HAM in the absence of serum (a) or the presence of 2% (b) or 10% (c) FBS or 2% (d) PRP. The scale bar indicates 200 μm. (B) Cells were seeded into 96 well plates and incubated in DMEM/F12-HAM containing 20% FBS for 24 hr. The culture medium was then replaced with DMEM/F12-HAM in the absence of serum (control) or presence of 2% FBS or 10% FBS or 2% PRP. After 3 days in CO_2 incubator, the cell number in each well was examined by DNA content in comparison to those on day 0 (open bar). The values for the serum (-), 10% FBS, and 2% PRP groups were significantly different compared with those on Day 0 ($^*P < 0.05$). (C) The cell numbers were examined in wells cultured in DMEM/F12-HAM containing various concentrations of PRP (circle), FBS (triangle), and PPP (square) after 3 days of culture similarly as Figure 2B. The growth stimulatory effect was not significantly different between 10% and 20% FBS and PPP (data not shown).

PRP inhibits the apoptosis of ccdPAs

The high proliferation-inducing property of PRP for ccdPAs in culture prompted us to further analyze PRP for protective effects against apoptosis in ccdPAs, since PRP is rich in cytokines and proteinases involved not only in proliferation, but also in regulating apoptosis (Eppley *et al.*, 2004, 2006; Foster *et al.*, 2009; Redler *et al.*, 2011). The protection of the cells from death may contribute to their longer survival after transplantation, together with a high potential for proliferation. To investigate the possibility, the ccdPAs (1×10^6 cells) were seeded and incubated in a 10 cm dish with DMEM/HAM medium containing 20% FBS for 16 hr, and subsequently incubated with the medium with or without 2% FBS, 2% PRP, or 2% PPP. After incubation for 8 hr, the cells were collected and stained with Annexin V-FITC. The flow cytometric analysis showed that 5.5% of cells were identified as Annexin V positive in the medium without serum (Figure 3A). The number of apoptotic cells was significantly decreased in the media with 2% FBS, 2% PRP, or 2% PPP in comparison to that in the cells cultured in serum-free medium. Among the various supplements, 2% PRP drastically reduced the number of apoptotic cells in comparison to 2% FBS or 2% PPP. ERK1/2 phosphorylation was examined to further analyze the protective effect of PRP against apoptosis, because the activation of the

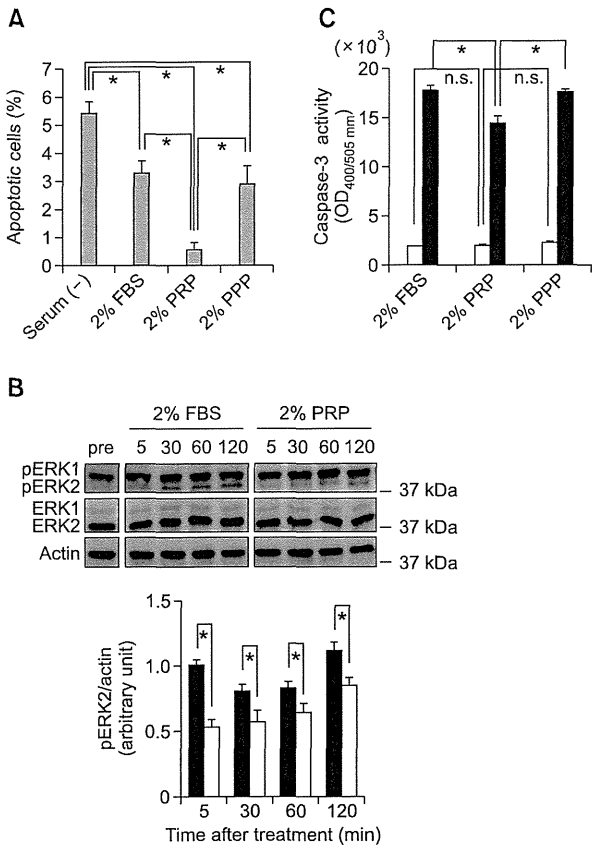

Figure 3. PRP decreased the apoptotic cell death and caspase 3 activity induced by TNF-α and cycloheximide in ccdPAs. (A) ccdPAs were seeded and incubated for 16 hr with medium containing 20% FBS, and the medium was then replaced with fresh medium without serum (Serum (-)) or with media containing 2% PRP, FBS, or PPP, and the cells were subsequently incubated at 37°C for 8 hr. The cells were then collected, stained by Annexin V-FITC and propidium iodide (PI), and analyzed using a Tali™ Image Based Cytometer (Life technologies). FITC-positive/PI-negative cells were considered to be apoptotic cells. *$P < 0.05$. (B) After incubation for 16 hr with medium containing 20% FBS, ccdPAs were pretreated for 2 hr with the medium containing 2% PRP or FBS. The cells were treated with TNF-α and cycloheximide for 5, 30, 60, and 120 min in the medium with 2% FBS (closed bar) or 2% PRP (open bar). Cell lysates were prepared at each time point as well as pretreatment (pre) and then were subjected to an immunoblot analysis of phosphorylated or unphosphorylated form of ERK1/2, and Actin. Results of densitometric analysis of phosphorylated form of ERK2 (pERK2) is shown below. After normalization of signals of pERK2 by Actin, each value of pERK2 was expressed as the fold increase of that at 5 min with 2% FBS. *$P < 0.05$. (C) After pretreatment for 2 hr with the medium containing 2% PRP, FBS, or PPP, the cells were incubated for 3 hr in the absence (open bars) or presence (closed bars) of TNF-α and cycloheximide, which induce apoptotic cell death. The caspase-3 activity in the lysates of collected cells were measured. *$P < 0.05$.

cascade is important for apoptosis *via* various intracellular signals including TNF-α (Cawthorn and Sethi, 2008; Mebratu and Tesfaigzi, 2009; Cagnol and Chambard, 2010). The cells were incubated with 2% PRP, FBS, or PPP for 2 hr, and apoptosis was induced by TNF-α and cycloheximide. Phosphorylation was detected following treatment with TNF-α and cycloheximide for 5 min in the cells cultured with 2% FBS. A densitometric analysis showed the amount of phosphorylated ERK2, and not phosphorylated ERK1, to significantly decrease in the medium with 2% PRP in comparison to the medium with 2% FBS (Figure 3B). The caspase-3 activity induced by TNF-α and cycloheximide for 3 hr were also significantly decreased in ccdPAs in the medium with 2% PRP in comparison to the cells cultured with 2% FBS or 2% PPP (Figure 3C). Thus, the apoptosis of ccdPAs was inhibited by culturing them in the medium with 2% PRP *in vitro*.

PRP almost completely inhibits the expression of the pro-apoptotic genes, DAPK1 and BIM, in ccdPAs after serum starvation

In order to identify the molecules involved in the anti-apoptotic effects of PRP on ccdPAs in culture, the expression profiles of representative apoptosis-related genes were examined using a PCR array profiler. The cells (2.5×10^5 cells) were seeded into 10 cm dishes and incubated in DMEM/HAM containing 20% FBS for 16 hr. The media was replaced with DMEM/HAM containing 2% PRP or FBS, the cells were incubated for 3 days, and the total RNA was isolated from the cultured cells to analyze the expression of apoptosis-related genes. Two independent experiments showed that, among the 84 genes examined, there were 8 genes with a more than 2-fold increase in expression, and 9 genes with a more than 2-fold decrease in expression in the cells cultured in the medium with 2% PRP compared with those cultured in the medium with 2% FBS (Table 1). We focused our interest on two genes, DAPK1 (reduced to 7.4% of the expression level observed with FBS) and BCL2L11 (also called BIM, reduced to 18.9% of the level observed with FBS), as representative genes with the obvious downregulation in the medium with 2% PRP (Figure 4). DAPK1 and BIM have been shown to be one of master regulators of cell death (Gozuacik and Kimchi, 2006), and is essential for BAX-dependent cell death (Kim *et al.*, 2009; Ren *et al.*, 2010), respectively.

The role of DAPK1 and BIM genes in apoptosis of preadipocytes was investigated by examining the effect of serum starvation of cells incubated with PRP on the expressions of these genes. The ccdPAs (2.5×10^5 cells) were seeded into 10 cm dishes and incubated in DMEM/HAM containing 20% FBS for 16 hr. The medium was replaced by medium containing 10% FBS (control), 2% FBS, 2% PRP, or 2% PPP, the cells were cultured for 3 days and the expression of DAPK1 and BIM were

Table 1. Apoptosis-related genes affected by PRP

Unigene	Refseq	Symbol	Description	Fold change
Downregulated				
Hs.380277	NM_004938	DAPK1	Death-associated protein kinase 1	13.5803 ↓
Hs.469658	NM_006538	BCL2L11	BCL2-like 11 (apoptosis facilitator)	5.2596 ↓
Hs.5353	NM_001230	CASP10	Caspase 10, apoptosis-related cysteine peptidase	4.0726 ↓
Hs.591834	NM_003844	TNFRSF10A	Tumor necrosis factor receptor superfamily, member 10a	3.967 ↓
Hs.513667	NM_003946	NOL3	Nucleolar protein 3 (apoptosis repressor with CARD domain)	2.8887 ↓
Hs.501497	NM_001252	CD70	CD70 molecule	2.8129 ↓
Hs.87247	NM_003806	HRK	Harakiri, BCL2 interacting protein (contains only BH3 domain)	2.5816 ↓
Hs.710305	NM_004536	NAIP	NLR family, apoptosis inhibitory protein	2.3876 ↓
Hs.643120	NM_000875	IGF1R	Insulin-like growth factor 1 receptor	2.1732 ↓
Upregulated				
Hs.127799	NM_001165	BIRC3	Baculoviral IAP repeat-containing 3	10.851 ↑
Hs.462529	NM_003790	TNFRSF25	Tumor necrosis factor receptor superfamily, member 25	4.0981 ↑
Hs.478275	NM_003810	TNFSF10	Tumor necrosis factor (ligand) superfamily, member 10	4.0907 ↑
Hs.654459	NM_001561	TNFRSF9	Tumor necrosis factor receptor superfamily, member 9	2.9875 ↑
Hs.522506	NM_021138	TRAF2	TNF receptor-associated factor 2	2.8331 ↑
Hs.9216	NM_001227	CASP7	Caspase 7, apoptosis-related cysteine peptidase	2.2033 ↑
Hs.145726	NM_001205	BNIP1	BCL2/adenovirus E1B 19kDa interacting protein 1	2.0258 ↑
Hs.194726	NM_004874	BAG4	BCL2-associated athanogene 4	2.0241 ↑

Genes identified as having a change in expression > 2-fold induced by the addition of PRP in comparison to 2% FBS are shown.

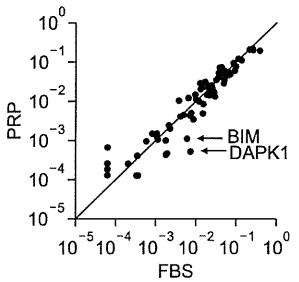

Figure 4. The results of the analysis of the expression of apoptosis-related genes affected by PRP. Total RNA was extracted from the cells cultured in the presence of 2% FBS or 2% PRP for 72 hr. The total RNA was subjected to cDNA synthesis and subsequent quantification of the mRNA expression for various apoptosis-related genes. The fold-changes in the quantified mRNA amounts compared to the average value of house-keeping genes were plotted for each gene (x-axis; cultured in 2% FBS, y-axis; cultured in 2% PRP).

analyzed. The DAPK1 mRNA level was increased 10.6-fold by serum starvation in comparison to the level in the cells cultured with 10% FBS, and the mRNA level was decreased to that of 10% FBS by the presence of 2% PRP. It is worth noting that, although the mRNA levels of DAPK1 in the cells cultured with 2% FBS and 2% PPP significantly decreased in comparison to those cultured without serum, the reductions were by 20.4% and 11.9%, respectively, which were less than that (93.6%) induced by culture in 2% PRP. The BIM mRNA levels were also drastically increased in the cells cultured in serum free medium in comparison to those cultured in the medium with 10% FBS (Figure 2C). The mRNA levels were reduced to those observed in the cells cultured with 10% FBS by the addition of 2% PRP. Again, the potential of 2% PRP to inhibit the mRNA expression of the target gene (by 87.2%) was significantly higher than that of the 2% FBS (54.1%) or 2% PPP (72.2%). Thus, PRP almost completely inhibited the expression of apoptosis-related genes induced by serum starvation.

Discussion

PRP inhibited the volume reduction of the 3D gels embedded with ccdPAs, the homogeneous preadipocytes, in comparison to the same concentration of FBS, and this was accompanied by increased cell viability in the gel. These observations prompted us to analyze the effects of PRP on the apoptosis and proliferation of the ccdPAs. The results showed that 2% PRP had a higher inhibitory effect on the apoptotic cell death of ccdPAs than 2% FBS or 2% PPP (Figure 3). A comparison between 2% PRP and 2% FBS by a gene expression profile analysis revealed that PRP downregulated 11% of the 84 representative apoptosis-related genes and upregulated 10% of the 84 representative apoptosis-related genes (Figure 4 and Table 1). The most drastically reduced genes were DAPK1, the protein product of which plays important roles in a wide range of signal transduction pathways with diverse outcomes, such as apoptosis, autoph-

agy and immune responses (Lin *et al.*, 2010), and BIM, encoding one of the BH3-only proteins, which is a critical regulator of apoptosis in many cell types (Ramesh *et al.*, 2009). The induction of these genes by apoptotic stimuli was almost completely prevented in the presence of PRP (Figure 5).

PRP, a concentrate of physiological cytokines, has been widely utilized as an injectable material in the clinic since the 1970s to enhance soft and hard tissue healing (Andia *et al.*, 2010; Lopez-Vidriero *et al.*, 2010; Redler *et al.*, 2011; Yu *et al.*, 2011), mainly by stimulating cell proliferation and angiogenesis in the injured tissues. PRP promotes the growth of various cells, including tissue-derived progenitor cells (Liu *et al.*, 2002; Lucarelli *et al.*, 2003; Doucet *et al.*, 2005; Frechette *et al.*, 2005; Vogel *et al.*, 2006; Kakudo *et al.*, 2008; Kurita *et al.*, 2008; Cervelli *et al.*, 2009; Chieregato *et al.*, 2011), and increases the revascularization of the transplanted tissues (Bir *et al.*, 2009). Based on these findings, the clinical applications of PRP have been broadened to recommend its use as an additive to tissue/cell transplantation therapies in plastic and reconstructive surgeries, and more recently in regenerative medicine. In fact, PRP has been shown to improve the fat graft survival (Abuzeni and Alexander, 2001; Sadati *et al.*, 2006; Cervelli *et al.*, 2009; Nakamura *et al.*, 2010; Pires Fraga *et al.*, 2010; Oh *et al.*, 2011) and bone and periodontal regenerations *via* cell transplantation (Tobita *et al.*, 2008; Chen *et al.*, 2010; Yamada *et al.*, 2010; Arvidson *et al.*, 2011).

In order to apply PRP for clinical transplantation therapy using preadipocytes cultured *in vitro*, it is necessary to elucidate the effects of PRP on cell survival in the grafts. However, the mechanisms by which PRP increases graft survival have not been well-characterized so far. The current study showed that PRP strongly induces the proliferation of ccdPAs, preadipocytes which were previously shown to be more adipogenic than ASCs (Asada *et al.*, 2011), compared with FBS at an equivalent concentration. Vogel *et al.* (2006) described that, because the addition of 2% PRP did not result in sufficient thrombocyte-clot formation to maintain a clot in the medium, a higher concentration of PRP, 3%, was evaluated for the stimulation of the MSC proliferation. In this study, to evaluate the efficacy of lower concentrations of PRP, the PRP was activated by thrombin to release cytokines (Aiba-Kojima *et al.*, 2007) prior to the experiments. As a result, 2% PRP showed almost the same effects on proliferation as 10% PRP, indicating its usability as a substitute for FBS in the expansion of preadipocytes for clinical applications. Finally, 2% PRP showed anti-apoptotic activities on the

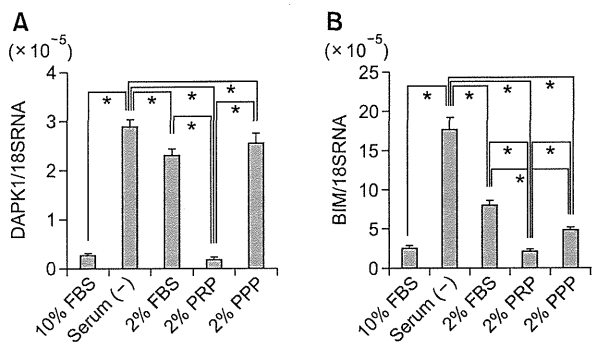

Figure 5. Serum starvation induced the expression of the DAPK1 and BIM genes, which was prevented by culture with 2% PRP. The ccdPAs were seeded and incubated for 16 hr in DMEM/HAM containing 20% FBS, and the culture medium was then replaced with medium without serum (Serum (-)), or with 2% or 10% FBS, 2% PRP, or 2% PPP, followed by incubation for an additional 72 hr. Quantitative reverse transcription-polymerase chain reaction (RT-PCR) was performed to evaluate the mRNA expression levels of DAPK1 (A) and BIM (B). The quantification of the given genes was expressed as relative mRNA level compared with a control after normalization to 18S RNA. $^*P < 0.05$.

preadipocytes, providing evidence that it can be used as an efficacious additive in the cell transplantation cocktail.

We observed that the expression of the DAPK1 and BIM genes was substantially upregulated by serum starvation in ccdPAs. However, the addition of PRP in the growth media effectively inhibited the apoptosis and downregulated the expression of these genes. TGF-β has been shown to induce the expression of DAPK1 and BIM, and to lead to subsequent apoptosis in other cell types (Jang *et al.*, 2002; Wildey *et al.*, 2003; Ramjaun *et al.*, 2007; Yu *et al.*, 2008). PRP may therefore inhibit the TGF-β-induced apoptosis cascade(s) during serum starvation in ccdPAs. Further analyses are needed to elucidate the mechanism(s) underlying the inhibitory potential of PRP on the expression levels of the representative apoptotic genes. The gene expression analysis also showed that PRP regulated the expression levels of genes involved in TNF signaling (TNFRSF10A, TNFRSF25, TNFSF10, TNFRSF9, and TRAF2), and of the Bcl protein superfamily, with its related proteins (HRK, BNIP1, and BAG4) (Table 1). The changes in the expression of these genes may also improve the survival of ccdPAs by modulating the apoptotic stimuli, considering that TNF-α signaling plays an important role in the regulation of the adipose tissue mass (Warne, 2003).

In conclusion, PRP inhibits cell apoptosis as well as or better than FBS, and also promotes the proliferation of the ccdPAs. The gene expression analyses identified that the DAPK1 and BIM genes were the most highly downregulated apoptosis-related

genes by PRP treatment in the preadipocytes. The identified characteristics of PRP with regard to the preadipocytes have advantages including increases in the cell number and improved cell survival in the transplanted grafts. Together with our findings for the efficacies of fibrin scaffold in transplantation of ccdPAs (Aoyagi *et al.*, 2011), the use of PRP for cell preparation and implantation of fat tissues and/or propagated cells may provide the graft with stable long-term survival after auto-transplantation.

Methods

Cell culture

Subcutaneous adipose tissues were obtained from healthy donors after informed consent was obtained, with approval from the ethics committee of Chiba University School of Medicine, and all studies were performed according to the guidelines of the Declaration of Helsinki. The preparation of the ceiling culture-derived proliferative adipocytes (ccdPAs) was performed as described previously (Kuroda *et al.*, 2011). Dulbecco's modified Eagle's medium/F12-HAM (DMEM/HAM, Sigma-Aldrich, St. Louis, MO) supplemented with 20% fetal bovine serum (FBS, SAFC Biosciences, Lenexa, KS) and 40 μg/ml gentamicin (GENTACIN, Schering-Plough Co., Kenilworth, NJ) was used as the culture media, unless otherwise noted in the text.

Preparation of PRP

Human PRP and PPP were prepared from healthy donors as follows; 52 ml of blood was obtained from the donors and mixed with 8 ml of Anticoagulant Citrate Dextrose Solution Formula A (ACD-A, TERUMO, Tokyo, Japan) solution, and transferred to 15 ml tubes. The tubes were centrifuged at 300 × *g* for 15 min at 20°C. The plasma and the buffy coat below the plasma were collected and transferred to new tubes. Secondary centrifugation was performed at 2000 × *g* for 15 min at 20°C. The clear supernatant (plasma) was decanted off until 6 ml was left and the middle portion of supernatant (plasma) was taken to be used as PPP. Finally, the remaining supernatant including the buffy coat was taken to be used as PRP. The platelet number of each product was automatically measured (XS 800i, sysmex Japan). The PRP utilized in this study contained 8.6×10^6 platelets/μl, which was approximately 7-fold concentrated from the original concentration in whole human plasma. Preparations of serum lysates containing platelet-released growth factors were essentially performed according to the method described by Aiba-Kojima *et al.* (2007). In brief, 2 U/ml of thrombin (Astellas Pharma Inc. Tokyo, Japan) was added to PRP and PPP, and the samples were agitated for 1 hr at 37°C and then incubated overnight at 4°C. Platelet bodies and any remaining fibrin were eliminated by centrifugation (2000 × *g* for 10 min), and the supernatants were obtained for the PRP and PPP. The serum samples were frozen at -20°C and thawed at 37°C before use. The growth medium was supplemented with 2 U/ml of heparin (Novo-Heparin, 5,000 units/5 ml for Injection, Mochida Pharm. Co. Tokyo, Japan).

Culture on fibrin scaffolds

Bolheal (The Chemo-Sero-Therapeutic Research Institute, Kumamoto, Japan) was used as a clinically available material to generate the fibrin gel. Fibrinogen and thrombin solutions were diluted with Ringer's Solution (Fuso Pharmaceutical Industries, Osaka, Japan) containing 0.5% human serum albumin (Mitsubishi Tanabe Pharma., Tokyo, Japan). The ccdPAs were suspended at 1×10^7 cells/ml by the diluted fibrinogen and thrombin solution. The final concentration of fibrinogen was 4 mg/ml and the thrombin solution was used at 1 U/ml. To form fibrin clots, 50 μl of the cell-fibrinogen suspension was added to each cell culture insert (Falcon 3104; Becton Dickinson, Franklin Lakes, NJ), then shortly thereafter, 50 μl of the cell-thrombin suspension was added into the insert, mixed by pipetting, and incubated at room temperature for 2 h. The inserts with fibrin clots were put on 12 well culture plates, and culture media were added to the inserts and wells. The plates were incubated at 37°C for 12 h in a 5% CO_2 incubator, and the media were replaced by fresh media containing FBS or PRP.

LDH assay

LDH released into the culture supernatant from the FG/ccdPA was measured using the CytoTox-One Homogeneous Membrane Integrity Assay kit (Promega, Madison, WI). A 100 μl sample of each culture supernatant was collected and added into to a 96-well plate. An equal volume of CytoTox-One Reagent was added and incubated for 10 min. Fifty μl of Stop Solution was added and the sample fluorescence was measured on a fluorescence microplate reader (SPECTRA max GEMINI XPS, Molecular Devices, Carlsbad, CA) using a wavelength of 560 nm/590 nm for excitation/emission. The original culture medium before the serum concentration was changed served as a pre-treatment control sample and the control value was subtracted from the value obtained after incubation with the medium containing different concentrations of serum.

Cell proliferation assay

The cell proliferation was examined using the CyQUANT^R Cell Proliferation Assay Kit (Life Technologies, Carlsbad, CA). Cells were seeded into 96 well plates at a density of 2×10^3 cells per well with DMEM/HAM/20% FBS. After 24 h, the culture medium was removed and changed to fresh DMEM/HAM without serum, or with FBS, PRP or PPP. After 3 days, the microplates were gently inverted and blotted onto paper towels to remove the medium from the wells. The microplates were then frozen and stored at -80°C and thawed at room temperature prior to analysis. CyQUANT GR dye/cell-lysis buffer was added to each well. Cells were incubated at room temperature for 5 min and the sample fluorescence was measured on a fluorescence microplate reader (SPECTRA max GEMINI XPS, Molecular Devices) using wavelength of 480 nm/520 nm for excitation/emission.

Induction of apoptosis, and the annexin V binding and caspase 3 activity assays

The cells were seeded into 10 cm dishes at a density of 1×10^6 cells per well with DMEM/HAM/20%FBS. After 24 h, the culture medium was removed and changed to fresh DMEM/HAM with 2% FBS, 2% PRP or 2%PPP. After 2 h, apoptosis was induced by the addition of 100 ng/ml TNF-α (Peprotech, Rocky Hill, NJ) and 100 μg/ml cycloheximide (CHX, Sigma-Aldrich). After 3 h, the culture supernatant was collected, and the cells were detached by TrypZean treatment. The detached cells were suspended in the collected culture supernatant. Subsequently, the cells were stained with Annexin V-FITC using a Tali™ Apoptosis kit (Life Technologies). Stained cells were analyzed by a Tali™ Image Based Cytometer (Life technologies). Cell lysates at the concentration of 1×10^4 cells/μl were prepared from the cells treated to induce apoptosis, and the caspase 3 activity levels were measured by a caspase-3/CPP32 Fluorometric Assay Kit (Biovision, Mountain View, CA). To examine the phosphorylation status of ERK1/2, the cells were scraped off at each time point in PBS and washed. The cells were pelleted and lysed by RIPA buffer (Wako Pure Chemical Industries, Ltd. Osaka, Japan), and the protein concentration was determined by Quant-iT Protein Assay Kit (Life technologies), and 5 μg of protein were analyzed by Western blotting using anti-ERK1 and anti-ERK1/2 (pT202/pY204) as primary antibodies (BD Biosciences, Franklin Lakes, NJ). Mouse TrueBlot ULTRA HRP-conjugated Anti-Mouse IgG (eBioscience, Inc. San Diego, CA) was used as a secondary antibody, and the signals were detected by SuperSignal® West Femto Maximum Sensitivity Substrate (Thermo Fisher Scientific Inc.) with LAS1000 apparatus (FUJI film, Tokyo, Japan). ERK signals were normalized using Actin signals detected by Anti-Actin monoclonal antibody (clone AC-40, Sigma-Aldrich).

Gene expression analysis

Cells (2.5×10^5 cells) were seeded into 10 cm dish with DMEM/HAM/20% FBS and cultured for 16 h. The culture medium was changed to fresh DMEM/HAM supplemented with 2% FBS or 2% PRP, and the cells were further incubated for 72 h. The total RNA from cultured cells was extracted using a RT^2 RNA Isolation Kit (SA Bioscience, Frederick, MD). Complementary DNA was generated from 1 μg of total RNA using the RT^2 First Strand Kit. An Apoptosis Reverse Transcriptase RT^2 profiler PCR array and RT^2 Real-Time SYBR Green/ROX PCR Mix (SA Bioscience, Frederick, MD) were used to identify the genes affected by PRP according to manufacturer's instruction. The data were analyzed by web-based data analysis software provided by the manufacturer. The probe and primer sets used to quantify the mRNA for the DAPK1 and BIM genes were purchased from Applied Biosystems (Life Technologies). The quantification of given genes was expressed as the relative mRNA level compared with a control after normalization to 18S RNA. All the real-time PCR were performed using an ABI 7500 real-time PCR apparatus.

Statistical analysis

The data are presented as the means ± S.D. Statistical comparisons were made by Student's *t*-test or an ANOVA followed by the post-hoc Tukey test using the SPSS software program. In all cases, *P*-values < 0.05 were considered to be significant.

Acknowledgements

We thank Dr. Fumiaki Matsumoto, Mr. Shunichi Konno, Dr. Shigeaki Tanaka, and Mr. Masayuki Aso for helpful and valuable suggestions about our research. This study was supported by Health and Labour Sciences Research Grants for Translational Research, Japan (H. B.), and in part by the Global COE Program (Global Center for Education and Research in Immune System Regulation and Treatment), MEXT, Japan (Y.O., Y.N., and H.B.).

References

Abuzeni PZ, Alexander RW. Enhancement of autologous fat transplantation with platelet rich plasma. Am J Cosmet Surg 2001;18:59-70

Aiba-Kojima E, Tsuno NH, Inoue K, Matsumoto D, Shigeura T, Sato T, Suga H, Kato H, Nagase T, Gonda K, Koshima I, Takahashi K, Yoshimura K. Characterization of wound drainage fluids as a source of soluble factors associated with wound healing: comparison with platelet-rich plasma and potential use in cell culture. Wound Repair Regen 2007; 15:511-20

Andia I, Sanchez M, Maffulli N. Tendon healing and platelet-rich plasma therapies. Expert Opin Biol Ther 2010; 10:1415-26

Anitua E, Sanchez M, Nurden AT, Nurden P, Orive G, Andia I. New insights into and novel applications for platelet-rich fibrin therapies. Trends Biotechnol 2006;24:227-34

Aoyagi Y, Kuroda M, Asada S, Bujo H, Tanaka S, Konno S, Tanio M, Ishii I, Aso M, Saito Y. Fibrin glue increases the cell survival and the transduced gene product secretion of the ceiling culture-derived adipocytes transplanted in mice. Exp Mol Med 2011;43:161-7

Aoyagi Y, Kuroda M, Asada S, Tanaka S, Konno S, Tanio M, Aso M, Okamoto Y, Nakayama T, Saito Y, Bujo H. Fibrin grue is a candidate scaffold for long-term therapeutic protein expression in spontaneously differentiated adipocytes *in vitro*. Exp Cell Res 2012;318:8-15

Arvidson K, Abdallah BM, Applegate LA, Baldini N, Cenni E, Gomez-Barrena E, Granchi D, Kassem M, Konttinen YT, Mustafa K, Pioletti DP, Sillat T, Finne-Wistrand A. Bone regeneration and stem cells. J Cell Mol Med 2011;15:718-46

Asada S, Kuroda M, Aoyagi Y, Fukaya Y, Tanaka S, Konno S, Tanio M, Aso M, Satoh K, Okamoto Y, Nakayama T, Saito Y, Bujo H. Ceiling culture-derived proliferative adipocytes retain high adipogenic potential suitable for use as a vehicle for gene transduction therapy. Am J Physiol Cell Physiol 2011;301:C181-5

Bauer-Kreisel P, Goepferich A, Blunk T. Cell-delivery therapeutics for adipose tissue regeneration. Adv Drug Deliv Rev 2010;62:798-813

Bhanot S, Alex JC. Current applications of platelet gels in facial plastic surgery. Facial Plast Surg 2002;18:27-33

Billings E Jr, May JW Jr. Historical review and present status of free fat graft autotransplantation in plastic and reconstructive surgery. Plast Reconstr Surg 1989;83:368-81

Bir SC, Esaki J, Marui A, Yamahara K, Tsubota H, Ikeda T, Sakata R. Angiogenic properties of sustained release platelet-rich plasma: characterization in-vitro and in the ischemic hind limb of the mouse. J Vasc Surg 2009;50: 870-9.e2

Cagnol S, Chambard JC. ERK and cell death: mechanisms of ERK-induced cell death-apoptosis, autophagy and senescence. FEBS J 2010;277:2-21

Cawthorn WP, Sethi JK. TNF-a and adipocyte biology. FEBS Lett 2008;582:117-31

Cervelli V, Gentile P, Scioli MG, Grimaldi M, Casciani CU, Spagnoli LG, Orlandi A. Application of platelet-rich plasma in plastic surgery: clinical and *in vitro* evaluation. Tissue Eng Part C Methods 2009;15:625-34

Chen FM, Zhang J, Zhang M, An Y, Chen F, Wu ZF. A review on endogenous regenerative technology in periodontal regenerative medicine. Biomaterials 2010;31:7892-927

Chieregato K, Castegnaro S, Madeo D, Astori G, Pegoraro M, Rodeghiero F. Epidermal growth factor, basic fibroblast growth factor and platelet-derived growth factor-bb can substitute for fetal bovine serum and compete with human platelet-rich plasma in the ex *vivo* expansion of mesenchymal stromal cells derived from adipose tissue. Cytotherapy 2011; 13:933-43

Cho SW, Kim I, Kim SH, Rhie JW, Choi CY, Kim BS. Enhancement of adipose tissue formation by implantation of adipogenic-differentiated preadipocytes. Biochem Biophys Res Commun 2006;345:588-94

Doucet C, Ernou I, Zhang Y, Llense JR, Begot L, Holy X, Lataillade JJ. Platelet lysates promote mesenchymal stem cell expansion: a safety substitute for animal serum in cell-based therapy applications. J Cell Physiol 2005;205: 228-36

Eppley BL, Woodell JE, Higgins J. Platelet quantification and growth factor analysis from platelet-rich plasma: implications for wound healing. Plast Reconstr Surg 2004;114:1502-8

Eppley BL, Pietrzak WS, Blanton M. Platelet-rich plasma: a review of biology and applications in plastic surgery. Plast Reconstr Surg 2006;118:147e-59e

Foster TE, Puskas BL, Mandelbaum BR, Gerhardt MB, Rodeo SA. Platelet-rich plasma: from basic science to clinical applications. Am J Sports Med 2009;37:2259-72

Frechette JP, Martineau I, Gagnon G. Platelet-rich plasmas: growth factor content and roles in wound healing. J Dent Res 2005;84:434-9

Gimble JM, Katz AJ, Bunnell BA. Adipose-derived stem cells for regenerative medicine. Circ Res 2007;100:1249-60

Gozuacik D, Kimchi A. DAPk protein family and cancer. Autophagy 2006;2:74-9

Jang CW, Chen CH, Chen CC, Chen JY, Su YH, Chen RH. TGF-b induces apoptosis through Smad-mediated expression of DAP-kinase. Nat Cell Biol 2002;4:51-8

Kakudo N, Minakata T, Mitsui T, Kushida S, Notodihardjo FZ, Kusumoto K. Proliferation-promoting effect of platelet-rich plasma on human adipose-derived stem cells and human dermal fibroblasts. Plast Reconstr Surg 2008;122:1352-60

Kang YH, Jeon SH, Park JY, Chung JH, Choung YH, Choung HW, Kim ES, Choung PH. Platelet-rich fibrin is a Bioscaffold and reservoir of growth factors for tissue regeneration. Tissue Eng Part A 2011;17:349-59

Kim H, Tu HC, Ren D, Takeuchi O, Jeffers JR, Zambetti GP, Hsieh JJ, Cheng EH. Stepwise activation of BAX and BAK by tBID, BIM, and PUMA initiates mitochondrial apoptosis. Mol Cell 2009;36:487-99

Kimura Y, Ozeki M, Inamoto T, Tabata Y. Adipose tissue engineering based on human preadipocytes combined with gelatin microspheres containing basic fibroblast growth factor. Biomaterials 2003;24:2513-21

Kuramochi D, Unoki H, Bujo H, Kubota Y, Jiang M, Rikihisa N, Udagawa A, Yoshimoto S, Ichinose M, Saito Y. Matrix metalloproteinase 2 improves the transplanted adipocyte survival in mice. Eur J Clin Invest 2008;38:752-9

Kurita M, Aiba-Kojima E, Shigeura T, Matsumoto D, Suga H, Inoue K, Eto H, Kato H, Aoi N, Yoshimura K. Differential effects of three preparations of human serum on expansion of various types of human cells. Plast Reconstr Surg 2008;122:438-48

Kuroda M, Aoyagi Y, Asada S, Bujo H, Tanaka S, Konno S, Tanio M, Ishii I, Machida K, Matsumoto F, Satoh K, Aso M, Saito Y. Ceiling culture-derived proliferative adipocytes are a possible delivery vehicle for enzyme replacement therapy in lecithin: cholesterol acyltransferase deficiency. Open Gene Ther J 2011;4:1-10

Liu Y, Kalen A, Risto O, Wahlstrom O. Fibroblast proliferation due to exposure to a platelet concentrate *in vitro* is pH dependent. Wound Repair Regen 2002;10:336-40

Lin Y, Hupp TR, Stevens C. Death-associated protein kinase (DAPK) and signal transduction: additional roles beyond cell death. FEBS J 2010;277:48-57

Lopez-Vidriero E, Goulding KA, Simon DA, Sanchez M, Johnson DH. The use of platelet-rich plasma in arthroscopy and sports medicine: optimizing the healing environment. Arthroscopy 2010;26:269-78

Lucarelli E, Beccheroni A, Donati D, Sangiorgi L, Cenacchi A, Del Vento AM, Meotti C, Bertoja AZ, Giardino R, Fornasari PM, Mercuri M, Picci P. Platelet-derived growth factors enhance proliferation of human stromal stem cells. Biomaterials 2003;24:3095-100

Man D, Plosker H, Winland-Brown JE. The use of autologous platelet-rich plasma (platelet gel) and autologous platelet-poor plasma (fibrin glue) in cosmetic surgery. Plast Reconstr Surg 2001;107:229-37;discussion 238-9

Margolis DJ, Kantor J, Santanna J, Strom BL, Berlin JA.

Effectiveness of platelet releasate for the treatment of diabetic neuropathic foot ulcers. Diabetes Care 2001;24:483-8

Martinez-Zapata MJ, Marti-Carvajal A, Sola I, Bolibar I, Angel Exposito J, Rodriguez L, Garcia J. Efficacy and safety of the use of autologous plasma rich in platelets for tissue regeneration: a systematic review. Transfusion 2009;49: 44-56

Mebratu Y, Tesfaigzi Y. How ERK1/2 activation controls cell proliferation and cell death: Is subcellular localization the answer? Cell Cycle 2009;8:1168-75

Muller AM, Davenport M, Verrier S, Droeser R, Alini M, Bocelli-Tyndall C, Schaefer DJ, Martin I, Scherberich A. Platelet lysate as a serum substitute for 2D static and 3D perfusion culture of stromal vascular fraction cells from human adipose tissue. Tissue Eng Part A 2009;15:869-75

Nakamura S, Ishihara M, Takikawa M, Murakami K, Kishimoto S, Yanagibayashi S, Kubo S, Yamamoto N, Kiyosawa T. Platelet-rich plasma (PRP) promotes survival of fat-grafts in rats. Ann Plast Surg 2010;65:101-6

Ning H, Liu G, Lin G, Yang R, Lue TF, Lin CS. Fibroblast growth factor 2 promotes endothelial differentiation of adipose tissue-derived stem cells. J Sex Med 2009;6:967-79

Oh DS, Cheon YW, Jeon YR, Lew DH. Activated platelet-rich plasma improves fat graft survival in nude mice: a pilot study. Dermatol Surg 2011;37:619-25

Patrick CW Jr. Adipose tissue engineering: the future of breast and soft tissue reconstruction following tumor resection. Semin Surg Oncol 2000;19:302-11

Patrick CW Jr. Tissue engineering strategies for adipose tissue repair. Anat Rec 2001;263:361-6

Pires Fraga MF, Nishio RT, Ishikawa RS, Perin LF, Helene A Jr, Malheiros CA. Increased survival of free fat grafts with platelet-rich plasma in rabbits. J Plast Reconstr Aesthet Surg 2010;63:e818-22

Ramesh S, Wildey GM, Howe PH. Transforming growth factor b (TGFb)-induced apoptosis: the rise & fall of Bim. Cell Cycle 2009;8:11-7

Ramjaun AR, Tomlinson S, Eddaoudi A, Downward J. Upregulation of two BH3-only proteins, Bmf and Bim, during TGF beta-induced apoptosis. Oncogene 2007;26:970-81

Redler LH, Thompson SA, Hsu SH, Ahmad CS, Levine WN. Platelet-rich plasma therapy: a systematic literature review and evidence for clinical use. Phys Sportsmed 2011;39:42-51

Ren D, Tu HC, Kim H, Wang GX, Bean GR, Takeuchi O, Jeffers JR, Zambetti GP, Hsieh JJ, Cheng EH. BID, BIM, and PUMA are essential for activation of the BAX- and BAK-dependent cell death program. Science 2010;330:1390-3

Sadati KS, Corrado AC, Alexander RW. Platelet-rich plasma (PRP) utilized to promote greater graft volume retention in autologous fat grafting. Am J Cosmet Surg 2006;23:203-11

Sclafani AP. Applications of platelet-rich fibrin matrix in facial plastic surgery. Facial Plast Surg 2009;25:270-6

Stashower M, Smith K, Williams J, Skelton H. Stromal progenitor cells present within liposuction and reduction abdominoplasty fat for autologous transfer to aged skin. Dermatol Surg 1999;25:945-9

Sterodimas A, de Faria J, Nicaretta B, Pitanguy I. Tissue engineering with adipose-derived stem cells (ADSCs): current and future applications. J Plast Reconstr Aesthet Surg 2010;63:1886-92

Tobita M, Uysal AC, Ogawa R, Hyakusoku H, Mizuno H. Periodontal tissue regeneration with adipose-derived stem cells. Tissue Eng Part A 2008;14:945-53

Torio-Padron N, Borges J, Momeni A, Mueller MC, Tegtmeier FT, Stark GB. Implantation of VEGF transfected pre-adipocytes improves vascularization of fibrin implants on the cylinder chorioallantoic membrane (CAM) model. Minim Invasive Ther Allied Technol 2007;16:155-62

Vogel JP, Szalay K, Geiger F, Kramer M, Richter W, Kasten P. Platelet-rich plasma improves expansion of human mesenchymal stem cells and retains differentiation capacity and *in vivo* bone formation in calcium phosphate ceramics. Platelets 2006;17:462-9

Warne JP. Tumour necrosis factor a: a key regulator of adipose tissue mass. J Endocrinol 2003;177:351-5

Welsh WJ. Autologous platelet gel: clinical function and usage in plastic surgery. Cosmet Dermatol 2000;13:13-8

Wildey GM, Patil S, Howe PH. Smad3 potentiates transforming growth factor b (TGFβ)-induced apoptosis and expression of the BH3-only protein Bim in WEHI 231 B lymphocytes. J Biol Chem 2003;278:18069-77

Wu W, Zhang J, Dong Q, Liu Y, Mao T, Chen F. Platelet-rich plasma - A promising cell carrier for micro-invasive articular cartilage repair. Med Hypotheses 2009;72:455-7

Yamada Y, Nakamura S, Ito K, Sugito T, Yoshimi R, Nagasaka T, Ueda M. A feasibility of useful cell-based therapy by bone regeneration with deciduous tooth stem cells, dental pulp stem cells, or bone-marrow-derived mesenchymal stem cells for clinical study using tissue engineering technology. Tissue Eng Part A 2010;16:1891-900

Yamaguchi M, Matsumoto F, Bujo H, Shibasaki M, Takahashi K, Yoshimoto S, Ichinose M, Saito Y. Revascularization determines volume retention and gene expression by fat grafts in mice. Exp Biol Med (Maywood) 2005;230:742-8

Yoshimura K, Suga H, Eto H. Adipose-derived stem/progenitor cells: roles in adipose tissue remodeling and potential use for soft tissue augmentation. Regen Med 2009;4:265-73

Yu J, Zhang L, Chen A, Xiang G, Wang Y, Wu J, Mitchelson K, Cheng J, Zhou Y. Identification of the gene transcription and apoptosis mediated by TGF-β-Smad2/3-Smad4 signaling. J Cell Physiol 2008;215:422-33

Yu W, Wang J, Yin J. Platelet-rich plasma: a promising product for treatment of peripheral nerve regeneration after nerve injury. Int J Neurosci 2011;121:176-80

Zuk PA, Zhu M, Mizuno H, Huang J, Futrell JW, Katz AJ, Benhaim P, Lorenz HP, Hedrick MH. Multilineage cells from human adipose tissue: implications for cell-based therapies. Tissue Eng 2001;7:211-28

Arteriosclerosis, Thrombosis, and Vascular Biology

JOURNAL OF THE AMERICAN HEART ASSOCIATION

American Heart Association®

Liver-Specific Deletion of 3-Hydroxy-3-Methylglutaryl Coenzyme A Reductase Causes Hepatic Steatosis and Death

Shuichi Nagashima, Hiroaki Yagyu, Ken Ohashi, Fumiko Tazoe, Manabu Takahashi, Taichi Ohshiro, Tumenbayar Bayasgalan, Kenta Okada, Motohiro Sekiya, Jun-ichi Osuga and Shun Ishibashi

Arterioscler Thromb Vasc Biol. 2012;32:1824-1831; originally published online June 14, 2012;
doi: 10.1161/ATVBAHA.111.240754
Arteriosclerosis, Thrombosis, and Vascular Biology is published by the American Heart Association, 7272 Greenville Avenue, Dallas, TX 75231
Copyright © 2012 American Heart Association, Inc. All rights reserved.
Print ISSN: 1079-5642. Online ISSN: 1524-4636

The online version of this article, along with updated information and services, is located on the World Wide Web at:
http://atvb.ahajournals.org/content/32/8/1824

Data Supplement (unedited) at:
http://atvb.ahajournals.org/content/suppl/2012/06/14/ATVBAHA.111.240754.DC1.html

Permissions: Requests for permissions to reproduce figures, tables, or portions of articles originally published in *Arteriosclerosis, Thrombosis, and Vascular Biology* can be obtained via RightsLink, a service of the Copyright Clearance Center, not the Editorial Office. Once the online version of the published article for which permission is being requested is located, click Request Permissions in the middle column of the Web page under Services. Further information about this process is available in the Permissions and Rights Question and Answer document.

Reprints: Information about reprints can be found online at:
http://www.lww.com/reprints

Subscriptions: Information about subscribing to *Arteriosclerosis, Thrombosis, and Vascular Biology* is online at:
http://atvb.ahajournals.org//subscriptions/

Downloaded from http://atvb.ahajournals.org/ at Jichi Medical School on February 20, 2013

Liver-Specific Deletion of 3-Hydroxy-3-Methylglutaryl Coenzyme A Reductase Causes Hepatic Steatosis and Death

Shuichi Nagashima, Hiroaki Yagyu, Ken Ohashi, Fumiko Tazoe, Manabu Takahashi, Taichi Ohshiro, Tumenbayar Bayasgalan, Kenta Okada, Motohiro Sekiya, Jun-ichi Osuga, Shun Ishibashi

Objective—3-hydroxy-3-methylglutaryl coenzyme A reductase (HMGCR) catalyzes the rate-limiting step in cholesterol biosynthesis and has proven to be an effective target of lipid-lowering drugs, statins. The aim of this study was to understand the role of hepatic HMGCR in vivo.

Methods and Results—To disrupt the HMGCR gene in liver, we generated mice homozygous for a floxed HMGCR allele and heterozygous for a transgene encoding Cre recombinase under the control of the albumin promoter (liver-specific HMGCR knockout mice). Ninety-six percent of male and 71% of female mice died by 6 weeks of age, probably as a result of liver failure or hypoglycemia. At 5 weeks of age, liver-specific HMGCR knockout mice showed severe hepatic steatosis with apoptotic cells, hypercholesterolemia, and hypoglycemia. The hepatic steatosis and death were completely reversed by providing the animals with mevalonate, indicating its essential role in normal liver function. There was a modest decrease in hepatic cholesterol synthesis in liver-specific HMGCR knockout mice. Instead, they showed a robust increase in the fatty acid synthesis, independent of sterol regulatory element binding protein-1c.

Conclusion—Hepatocyte HMGCR is essential for the survival of mice, and its abrogation elicits hepatic steatosis with jaundice and hypoglycemia. **(*Arterioscler Thromb Vasc Biol.* 2012;32:1824-1831.)**

Key Words: cholesterol ■ liver ■ 3-hydroxy-3-methylglutaryl coenzyme A ■ fatty acids ■ knockout mouse

The mevalonate pathway produces isoprenoids that are essential for the diverse cellular functions ranging from cholesterol synthesis to growth control. The enzyme 3-hydroxy-3-methylglutaryl-coenzyme A reductase (HMGCR) (EC 1.1.1.34), which catalyzes the conversion of HMG-coenzyme A to mevalonate, is the rate-limiting enzyme in the mevalonate pathway.[1] Mammalian HMGCR is an integral high-mannose glycoprotein of the endoplasmic reticulum (ER).[2] Structurally, it is divided into 2 major domains: a C-terminal cytosol-facing domain that tetramerizes to form the active site and an N-terminal hydrophobic region that spans the ER membrane 8× and bears a single N-glycan. This membrane region is dispensable for the enzymatic activity but necessary for the metabolically controlled stability of the enzyme and sufficient to cause sterol-accelerated degradation of heterologous proteins. Within this region, transmembrane spans 2 through 6 bear significant sequence homology to the corresponding transmembrane spans of sterol regulatory element binding protein (SREBP) cleavage-activating protein (SCAP).[3]

To ensure a steady supply of mevalonate, the nonsterol and sterol end products of the mevalonate metabolism exert feedback regulatory effects on the activity of this enzyme through multivalent mechanisms, including inhibition of the transcription of its RNA, blocking of translation, and acceleration of the protein's degradation by a mechanism called ER-associated degradation, thereby regulating the amount of protein over a several hundred-fold range. ER-associated degradation of HMGCR requires the binding of Insig-1 to the sterol-sensing domain.[4] Despite the critical role of HMGCR in cholesterol biosynthesis, little is known about its relevance to diseases. Only recently, HMGCR has been identified as a determinant of plasma cholesterol levels.[5]

Inhibitors of HMGCR, statins, are potent cholesterol-lowering agents that have been widely used to prevent the occurrence of coronary heart disease and other atherosclerotic diseases.[6] The atheroprotective properties of statins are primarily because of the potent low-density lipoprotein (LDL)-cholesterol–lowering effect.[7] Statins have also been reported to exert cholesterol-independent, or so-called pleiotropic, effects that involve improving endothelial function and decreasing oxidative stress and vascular inflammation.[8] The benefits of statins extend beyond cardiovascular diseases and include a reduction in the risk of dementia, Alzheimer disease, ischemic stroke, osteoporosis, tumor growth, and viral infection. Most of these pleiotropic effects are mediated by an ability to block the synthesis of nonsterol isoprenoid intermediates. Statins have toxic effects in only a limited number of patients and are generally considered safe.

Received on: May 2, 2011; final version accepted on: April 30, 2012.

From the Division of Endocrinology and Metabolism, Department of Medicine, Jichi Medical University, Shimotsuke, Tochigi, Japan (S.N., H.Y., F.T., M.T., T.O., T.B., K. Okada, J.O., S.I.); and Department of Metabolic Diseases, Graduate School of Medicine, University of Tokyo, Tokyo, Japan (K. Ohashi, M.S.).

The online-only Data Supplement is available with this article at http://atvb.ahajournals.org/lookup/suppl/doi:10.1161/ATVBAHA.111.240754/-/DC1.

Correspondence to Shun Ishibashi, MD, PhD, Division of Endocrinology and Metabolism, Department of Medicine, Jichi Medical University, 3311-1 Yakushiji, Shimotsuke, Tochigi 329-0498, Japan. E-mail ishibash@jichi.ac.jp

© 2012 American Heart Association, Inc.

Arterioscler Thromb Vasc Biol **is available at http://atvb.ahajournals.org** **DOI: 10.1161/ATVBAHA.111.240754**

Downloaded from http://atvb.ahajournals.org/ at Jichi Medical School on February 20, 2013

To establish an animal model for investigating the mechanisms behind the effects, including toxicity of statins, we have generated HMGCR knockout (KO) mice lacking the enzyme throughout their bodies.[9] These mice die in a relatively early stage of embryonic development (ie, before E8.5). Because mice lacking squalene synthase, the first committed enzyme in the sterol pathway, die in the embryonic stage with apparent anomalies of the development of the central nervous system,[10] we took advantage of the tissue-specific gene targeting using the Cre-loxP system to generate mice lacking HMGCR in a liver-specific manner.

Materials and Methods

Liver-specific HMGCRKO (L-HMGCRKO) mice were generated by cross-breeding heterozygous floxed HMGCR (referred to as $HMGCR^{+/f}$; f denotes floxed) mice with transgenic mice expressing Cre recombinase under the control of albumin gene promoter (Alb-Cre).[11,12] All animal experiments were performed with the approval of the Institutional Animal Care and Research Advisory Committee at Jichi Medical University. For detailed protocols for the generation of L-HMGCRKO mice and other experimental procedures, please refer to the online-only Data Supplement.

Results

Because there were no differences in growth curves or metabolic parameters, such as plasma lipid and glucose levels, among the $HMGCR^{+/+}$ (wild-type), $HMGCR^{+/+}$ Alb-Cre (CRE), and $HMGCR^{f/f}$ (fHMGCR) mice, we used fHMGCR mice as a control. To determine whether the expression of the HMGCR gene was abrogated in the liver, we performed a Southern blot (Figure 1A), Northern blot (Figure 1B), and real-time polymerase chain reaction (Figure 1C). The Southern blot analysis shows that only the 6.3-kb wild-type allele and 7.7-kb floxed allele were observed in the DNA from liver in wild-type and fHMGCR mice, respectively. In L-HMGCRKO mice at 3 weeks, the liver contained predominantly the 12.0-kb KO allele (70% based on PhosphorImager analysis [BAS 200, Fujifilm, Tokyo, Japan]) and some residual floxed allele (30%). The mRNA expression of HMGCR in the liver of L-HMGCRKO mice was decreased to 30% of the fHMGCR mice at 3 weeks of age and to <10% at 4 and 5 weeks upon Northern blot analysis. The time-dependent abrogation of the mRNA expression of HMGCR was also confirmed by real-time polymerase chain reaction. Based on this method, the mRNA levels were decreased to only 2% of the fHMGCR mice at 4 and 5 weeks, although there were no significant differences in other organs (Figure IIA in the online-only Data Supplement). Immunoblot analysis showed that the amount of HMGCR protein in the liver of L-HMGCRKO mice was 15% of that in fHMGCR mice (Figure 1D). Despite the profound reduction in HMGCR at both the mRNA and protein levels, the HMGCR activity in the liver of L-HMGCRKO mice was decreased by only 44% compared with that in fHMGCR mice (Figure 1E). To determine whether HMGCR is specifically abrogated in the liver parenchymal cells of L-HMGCRKO mice, we separated parenchymal and nonparenchymal cells from the liver at 3 weeks of age by density-gradient centrifugation after liver perfusion with collagenase. The mRNA expression of HMGCR in the parenchymal cells of L-HMGCRKO mice was decreased by 70.6% compared with that in fHMGCR mice, whereas the mRNA expression of HMGCR in the nonparenchymal cells was not different between the fHMGCR and L-HMGCRKO mice at 3 weeks of age (Figure IIC in the

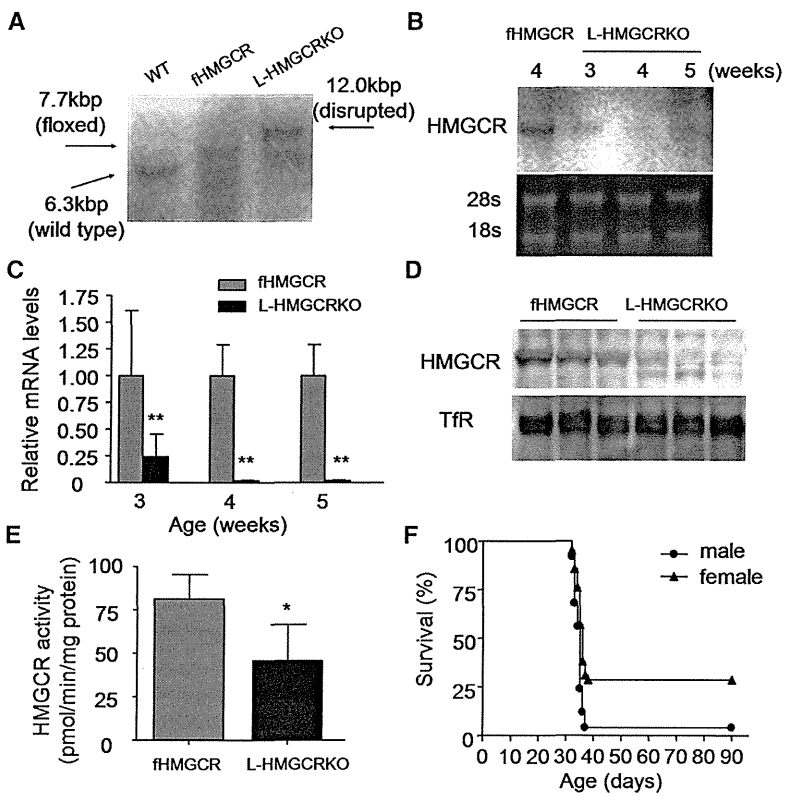

Figure 1. Conditional deletion of the 3-hydroxy-3-methylglutaryl-coenzyme A reductase (HMGCR) gene in mice and their survival. **A**, Southern blot analysis of *BamHI*-digested DNA from the livers of wild-type (WT) floxed HMGCR (fHMGCR) and liver-specific HMGCR knockout (L-HMGCRKO) mice at 3 weeks of age as described in the online-only Data Supplement. **B**, Northern blot analysis of hepatic RNA from the livers of fHMGCR and L-HMGCRKO mice at 3, 4, and 5 weeks of age. Aliquots (20 μg) of total RNA from liver were subjected to electrophoresis and blot hybridization with ^{32}P-labeled cDNA probes for mouse HMGCR as described in the online-only Data Supplement. **C**, Quantitative real-time polymerase chain reaction of HMGCR mRNA levels from the livers of mice indicated in **B** (n=5 in each group). **D**, Immunoblot analysis of HMGCR protein from the livers of control and L-HMGCRKO mice at 4 weeks of age (n=3 in each group). Aliquots (50 μg) of liver membrane fractions were subjected to SDS-PAGE and immunoblot analysis. The membrane protein transferrin receptor was used as a loading control. **E**, HMGCR activity in the liver microsomal fractions of fHMGCR and L-HMGCRKO mice at 4 weeks of age (n=5 in each group). **F**, The survival curves were generated by the Kaplan-Meier method, and differences among the survival rates were compared using the χ^2 method. Male (n=25) and female (n=42) L-HMGCRKO mice were followed for >100 days. Each value represents mean±SD. Significant differences compared with control mice: $^*P<0.05$ and $^{**}P<0.001$.

Downloaded from http://atvb.ahajournals.org/ at Jichi Medical School on February 20, 2013

Table. Liver Weight and Plasma Parameters of Control and L-HMGCRKO Mice

Age (wks)	3		4		5	
Genotype	fHMGCR (n=5)	L-HMGCRKO (n=5)	fHMGCR (n=9)	L-HMGCRKO (n=7)	fHMGCR (n=6)	L-HMGCRKO (n=5)
Body weight (g)	10.6±1.3	11.7±1.5	17.2±1.3	15.5±0.8*	21.7±2.0	13.5±0.8***
Liver weight (g)	0.47±0.11	0.51±0.11	0.78±0.14	0.92±0.13	1.08±0.11	1.17±0.28
Liver/body weight (%)	4.4±0.4	4.2±0.4	4.4±0.4	6.1±0.8*	5.0±0.12	8.7±2.1**
Total cholesterol (mg/dL)	63.6±9.1	47.1±1.0**	66.5±11.1	46.7±13.2**	64.6±6.8	282.6±72.6***
Free cholesterol (mg/dL)	26.2±4.0	20.1±0.5*	33.3±5.5	24.6±13.5	33.1±2.7	263.0±72.6***
Cholesterol ester (mg/dL)	37.4±5.5	27.0±1.4*	33.1±5.7	22.1±4.6*	31.5±4.9	19.6±10.3
Triglyceride (mg/dL)	62.5±13.3	51.1±9.9	78.5±25.4	24.9±6.9***	92.5±31.1	27.7±9.4**
Free fatty acids (mmol/L)	0.34±0.10	0.40±0.06	0.63±0.20	0.51±0.19	0.55±0.09	1.70±0.92*
Phospholipids (mg/dL)	132.2±20.2	106±2.7*	143.5±22.8	117.3±31.7	150.9±12.3	601.1±133.5**
Aspartate aminotransferase (IU/L)	76.1±10.2	95.7±45.5	92.7±39.3	343.1±602.8	55.9±18.6	1178.5±182.1***
Alanine transaminase (IU/L)	35.1±12.1	61.9±46.7	20.7±17.5	54.2±101.7	13.1±4.6	878.8±357.6**
Total bilirubin (mg/dL)	0.31±0.09	0.31±0.09	0.30±0.08	0.36±0.29	0.33±0.19	3.25±1.69*
Blood glucose (mg/dL)	110.6±16.7	123.0±15.5	115.9±13.7	99.6±16.7	135.7±9.4	48.3±23.3*

Blood samples were taken from male mice fed a normal chow diet ad libitum before the study. Each value represents the mean±SD. Significant differences compared with control mice: *P<0.05, **P<0.01, and ***P<0.001. HMGCR indicates 3-hydroxy-3-methylglutaryl-coenzyme A reductase; L-HMGCRKO, liver-specific HMGCR knockout mice; fHMGCR, floxed HMGCR.

online-only Data Supplement). HMGCR activity in the parenchymal cells of L-HMGCRKO mice was decreased by only 47% compared with that in fHMGCR mice (Figure IID in the online-only Data Supplement). The relative decreases in the mRNA and activity of HMGCR in the parencymal cells were similar to those observed in the whole liver of L-HMGCRKO mice (Figure 1C and E), supporting that HMGCR gene was specifically abrogated in the parenchymal cells of the liver and that there was no compensatory upregulation of HMGCR in the nonparenchymal cells of the L-HMGCRKO mice.

L-HMGCRKO mice were born at a rate in accordance with the rule of Mendelian inheritance. However, 96% of males died with a median survival time of 35 days, whereas 71% of females died with a median survival time of 36 days (Figure 1F), and the rest of them survived until 12 months of age. Therefore, the survival rate of females was significantly higher than males (P=0.025). The mRNA expression levels of HMGCR in the liver from the surviving HMGCRKO mice were as high as those from fHMGCR mice (Figure IIB in the online-only Data Supplement). Next, we compared body weight, liver weight, plasma lipid levels, liver functions, and blood glucose levels between fHMGCR and L-HMGCRKO mice (Table). Although the body weight of L-HMGCRKO mice was not different from that of fHMGCR mice at 3 weeks of age, it decreased by 10% at 4 weeks and by 38% at 5 weeks of age. Liver weight did not differ between the 2 groups. However, the ratio of liver weight to body weight was increased by 39% and 74% at 4 and 5 weeks of age, respectively. The livers of L-HMGCRKO mice were enlarged, paler, and whiter than those of fHMGCR mice at 5 weeks of age (Figure 2A and 2B). Consistent with the macroscopic abnormalities of the liver, plasma levels of aspartate aminotransferase, alanine transaminase, and bilirubin were markedly increased in the L-HMGCRKO mice compared with fHMGCR mice at 5 weeks of age. Total cholesterol levels in the plasma were decreased in the L-HMGCRKO mice by 26% at 3 weeks of age (Table). In parallel, plasma concentrations of LDL cholesterol and apolipoprotein (apo) B-100 protein were decreased (Figure IIIA and IIIE in the online-only Data Supplement). Despite the liver failure of L-HMGCRKO mice at 5 weeks of age, the plasma levels of cholesterol, free cholesterol, and phospholipids were increased 4.3-, 7.9-, and 4.0-fold, respectively. On the other hand, plasma cholesterol ester levels were decreased by 38% (Table). Therefore, calculated ratios of free cholesterol to cholesterol ester were increased 13-fold. Most of the increased cholesterol was distributed in the size of very low-density lipoprotein through LDL (Figure IIIC in the online-only Data Supplement). Although apoB-100 levels were decreased, apoB-48 levels were substantially increased in the plasma of L-HMGCRKO mice at 5 weeks of age (Figure IIIG in the online-only Data Supplement). These findings together with the results of agar gel electrophoresis of the plasma (Figure III-I in the online-only Data Supplement) strongly indicate that both lipoprotein X and apoB-48–containing lipoproteins were increased in the L-HMGCRKO mice. Hepatic LDL receptor protein levels were not altered between fHMGCR and L-HMGCRKO mice at 3 and 5 weeks of age (Figure IIIF and IIIH in the online-only Data Supplement), despite increased hepatic LDL receptor mRNA levels (Figure 4A). Plasma lipoprotein changes in L-HMGCRKO mice may not be influenced by LDL receptor protein levels. Plasma free fatty acid levels were also increased 3.1-fold at 5 weeks. In contrast, plasma triglyceride levels were decreased by 69% and 70% at 4 and 5 weeks of age, respectively. It is of note that L-HMRCRKO mice were moderately hypoglycemic at 5 weeks.

To determine the causes of the liver dysfunction associated with hepatomegaly, we performed a microscopic analysis of the liver (Figure 2). Hematoxylin and eosin staining revealed moderate to severe ballooning and unicellular necrosis of parenchymal cells at 5 weeks (Figure 2C and 2D). Oil-red O staining showed moderate to severe microvesicular steatosis of the parenchymal cells (Figure 2E and 2F). TdT-mediated dUTP-nick end labeling–positive (Figure 2G, 2H, and 2M) and Ki-67–positive parenchymal cells

Downloaded from http://atvb.ahajournals.org/ at Jichi Medical School on February 20, 2013

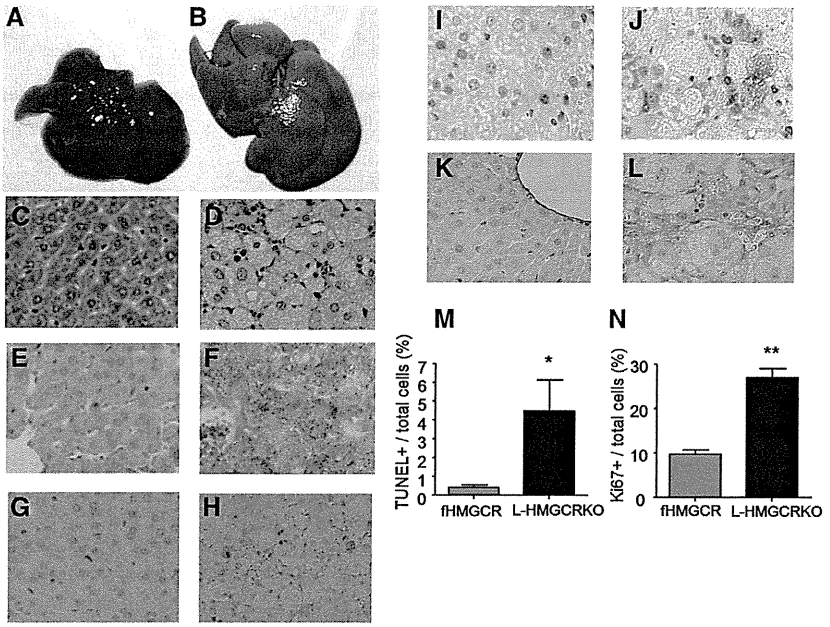

Figure 2. Gross appearance and histological analysis of the livers in male mice at 5 weeks. Gross appearance of the liver from control (**A**) and liver-specific HMGCR knockout (L-HMGCRKO) mice (**B**). Hematoxylin and eosin–stained liver sections from control (**C**) and L-HMGCRKO (**D**) mice. Frozen sections of liver stained with oil-red O from control (**E**) and L-HMGCRKO (**F**) mice. TdT-mediated dUTP-nick end labeling (TUNEL)–stained liver sections from control (**G**) and L-HMGCRKO (**H**) mice. Ki-67–stained liver sections from control (**I**) and L-HMGCRKO (**J**) mice. Type 4 collagen–stained liver sections from control (**K**) and L-HMGCRKO (**L**) mice. Bar graph shows the percentages of TUNEL-positive cells (**M**) and Ki-67–positive cells (**N**) relative to the total number of cells. Each value represents mean±SD. Significant differences compared with control mice: **P*<0.01 and ***P*<0.001.

(Figure 2I, 2J, and 2N) were significantly increased 11- and 2.8-fold in the liver of L-HMGCRKO mice compared with that in fHMGCR mice, respectively. The liver of L-HMGCRKO mice contained increased amounts of type 4 collagen (Figure 2K and 2L). Caspase 3 activity in the liver of L-HMGCRKO mice was also increased 1.8-fold compared with that of fHMGCR (Figure VA in the online-only Data Supplement). The mRNA levels of C/EBP-homologous protein were also significantly increased (Figure VD in the online-only Data Supplement). However, no significant differences were observed in either caspase 8 activity or H_2O_2 contents in the liver (Figure VB and VC in the online-only Data Supplement). The pathology of the liver from L-HMGCRKO mice at 4 weeks was milder (Figure IVB in the online-only Data Supplement) than that at 5 weeks. The liver of the mice which survived the lethal period still had hepatocyte ballooning (Figure IVD in the online-only Data Supplement).

To determine whether the liver-specific abrogation of HMGCR affected cholesterol metabolism in the liver, we measured the hepatic levels of cholesterol and triglycerides (Figure 3). The hepatic cholesterol content was decreased by only 22% in the L-HMGCRKO mice compared with the fHMGCR mice (Figure 3A). Unexpectedly, the hepatic contents of triglyceride were increased 2-fold (Figure 3B). These results indicate that the neutral lipids stained with oil-red O in the liver were primarily triglycerides. The reduction in the cholesterol contents of the liver was smaller than expected. We measured cholesterol synthesis in liver slices in culture (Figure 3C). The cholesterol synthesis was reduced by 45%. This reduction paralleled the degree of reduction in HMGCR activity in the liver (Figure 1E). We also measured the amounts of fatty acids synthesized in the liver (Figure 3D). Surprisingly, the synthesis of fatty acids from acetate was markedly increased 17-fold in the liver of L-HMGCRKO mice. Although total amounts of fatty acids were not different between the 2 mice (Figure 3E), the following fatty acid species were significantly increased in the liver of L-HMGCRKO mice: C18:0, C18:1n–9, C20:1n–9, C20:3n–9, and C22:4n–6 (Figure 3F). Given the increased production of fatty acids and triglycerides in the liver, we measured other metabolites of fatty acids such as diglycerides and ceramides. The hepatic levels of diglycerides were increased 1.8-fold (Figure 3G), but those of ceramides were not increased significantly (Figure 3H).

To clarify the mechanisms behind the changes in fatty acid metabolism, we determined the changes in the levels of mRNA expression in various genes involved in cholesterol or fatty acid metabolism in the liver at 4 weeks of age by real-time polymerase chain reaction (Figure 4A). As to the genes involved in cholesterol metabolism, the mRNA levels of SREBP2, LDL receptor, proprotein convertase subtilisin/kexin type 9, and squalene synthase were increased 1.4-, 1.9-, 2.8-, and 3.9-fold, respectively. On the other hand, the mRNA levels of cholesterol 7α-hydroxylase, a rate-limiting enzyme for bile acid synthesis, were decreased by 60%. With regard to the genes involved in fatty acid metabolism, the mRNA levels of fatty acid synthase (FAS), acetyl-CoA carboxylase, and stearoyl-CoA desaturase 2 were increased 2.4-, 1.4-, and 22-fold, respectively. On the other hand, the mRNA expression of SREBP1c and acyl CoA:diacylglycerol acyltransferase 2 was decreased by 80% and 40%, respectively. There were no changes in either the mRNA expression of SREBP1a, a splice variant of SREBP1c, or liver X receptor α (LXRα), an important transcriptional activator of the SREBP1c gene. The mRNA expression of peroxisome proliferator–activated receptor α, a transcription regulator of genes for fatty acid oxidation, was not changed.

HMGCR catalyzes the formation of mevalonate, which is used as a substrate for the synthesis not only of cholesterol but also nonsterols such as isoprenoids, ubiquinone, heme A, and dolichol. To test the notion that death, likely because of severe liver failure, was caused by the alteration of a nonsterol pathway, we evaluated the isoprenylation of small GTP-binding proteins such as H-Ras and Rac1 by measuring the amount of membrane-bound forms (Figure 4B). The ratio of the

Downloaded from http://atvb.ahajournals.org/ at Jichi Medical School on February 20, 2013

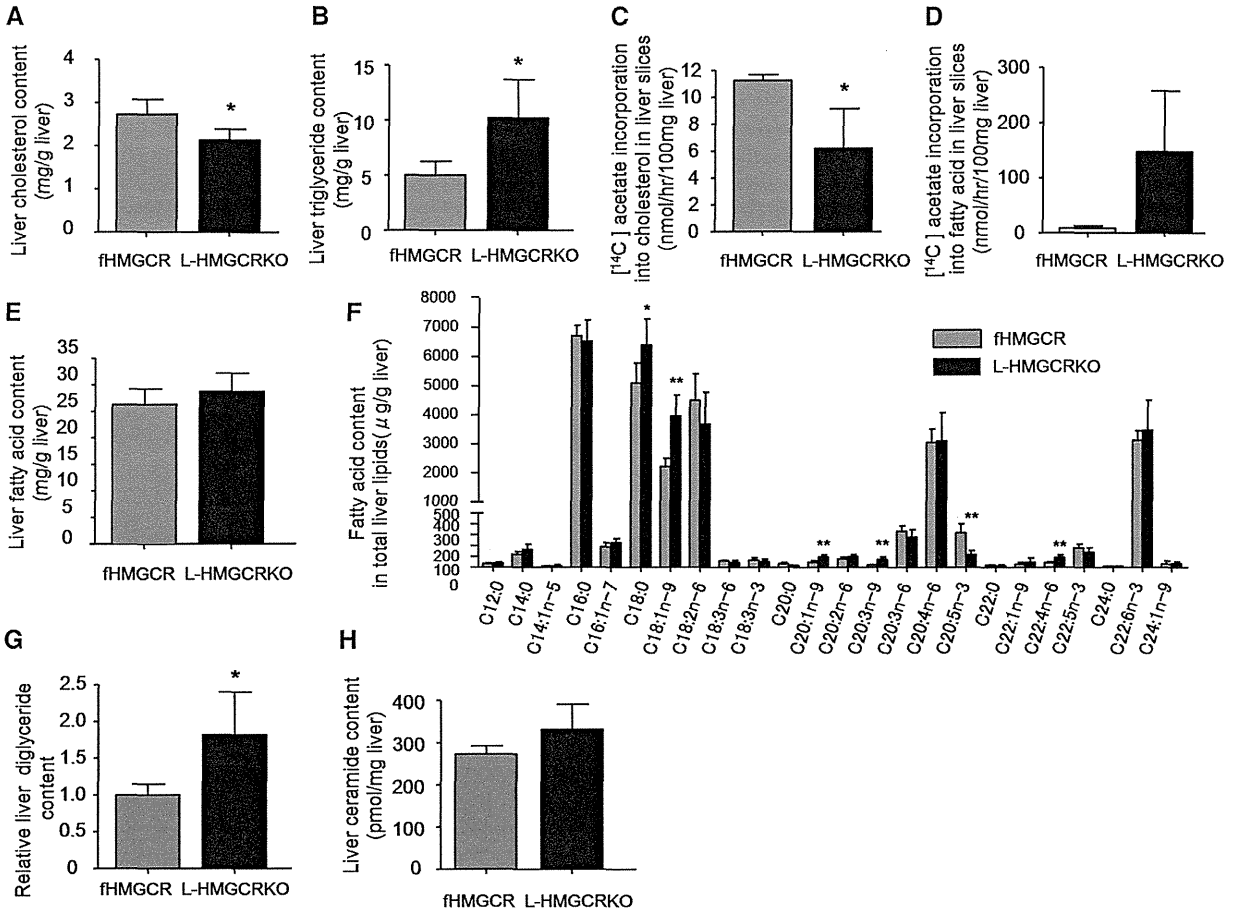

Figure 3. Hepatic lipid contents and lipid synthesis in the control and liver-specific HMGCR knockout (L-HMGCRKO) male mice. Hepatic total cholesterol (**A**), triglyceride (**B**), fatty acid levels (**E**), and fatty acid composition in total liver lipids (**F**) were determined in the livers from control and L-HMGCRKO mice at 4 weeks of age (n=5 in each group). **C** and **D**, In vitro hepatic lipid synthesis rate using the liver slices in culture (n=3 in control and n=4 in L-HMGCRKO). Liver slices (≈100 mg) were incubated with ^{14}C-labeled acetate (8 mmol/L, 0.1 μCi/μmol) for 90 minutes. After incubation, the slices were removed for measurement of ^{14}C-labeled cholesterol (**C**) and fatty acids (**D**). Hepatic diglyceride (**G**) and ceramide (**H**) contents were measured in the livers of control and L-HMGCRKO mice at 4 weeks of age (n=5 in each group) by the diglyceride kinase method as described in the online-only Data Supplement. Each value represents mean±SD. Significant differences compared with control mice: **P*<0.05 and ***P*<0.01.

membrane-bound form to the cytosolic form of H-Ras or Rac1 was decreased to 0.05 to 0.2 compared with control. These results indicate that the deficiency of HMGCR affected the nonsterol pathway more severely than the sterol pathway. We also estimated changes in intracellular signaling molecules (Figure 4C). p-Akt and c-Met were decreased by 72% and 81%, respectively, whereas phospho-signal transducer and activator of transcription 3 was increased 7.6-fold.

If the lethal phenotype of HMGCR deficiency is because of the deficiency of mevalonate, supplementation with mevalonate could theoretically rescue the lethal phenotype. In fact, providing the male mice with water containing mevalonate significantly attenuated the liver dysfunction and hypercholesterolemia (Figure 5A–5C). The pathological abnormalities observed in the male L-HMGCRKO mice were almost normalized by the supplementation with mevalonate (Figure 5D–5G). Consistently, the amounts of the membrane-bound form of H-Ras or Rac 1 were restored to normal levels (Figure 5H). Similar improvements were found in female L-HMGCRKO mice (data not shown). No death occurred until 40 days of age in L-HMGCRKO mice supplemented with mevalonate.

Because L-HMGCRKO mice were hypoglycemic (Table), it is possible that hypoglycemia is the direct cause of death. To test this hypothesis, we allowed mice free access to drinking water containing 20% (w/v) glucose. Glucose feeding significantly increased plasma glucose levels (43.5±16.2 mg/dL [n=10] versus 79.5±40.6 mg/dL [n=13] [*P*=0.01] in males; 36.6±13.3 mg/dL [n=4] versus 65.2±35.6 mg/dL [n=11] [*P*=0.04] in females). Concurrently, it dramatically improved the mortality of L-HMGCRKO mice (96% versus 13% in males and 71% versus 15% in females) (Figure VI in the online-only Data Supplement).

Discussion

Nearly all the male L-HMGCRKO mice died before 40 days of age, whereas 30% of females survived until 12 months of age. Before their death, the mice developed severe hepatic damage with hepatomegaly, steatosis, and hypoglycemia. Thus, we ascribe the lethal effect of the liver-specific deficiency of HMGCR

Downloaded from http://atvb.ahajournals.org/ at Jichi Medical School on February 20, 2013